Multilayer Stag Beetle elytra perform better under external loading via non-symmetric bending properties

Lakshminath Kundanati[1], Stefano Signetti[1]†, Himadri S. Gupta[2], Michele Menegon[3] and Nicola M. Pugno[1,2,4,*]

[1]*Laboratory of Bio-inspired and Graphene Nanomechanics, Department of Civil, Environmental and Mechanical Engineering, University of Trento, via Mesiano 77, I-38123 Trento*

[2]*School of Engineering and Materials Science, Queen Mary University of London, Mile End Road, E1 4NS London, United Kingdom*

[3]*MUSE Science Museum, corso del Lavoro e della Scienza 3, I-38122 Trento, Italy*

[4]*Ket-Lab, Edoardo Amaldi Foundation, Italian Space Agency, Via del Politecnico snc, I-00133 Rome, Italy*

Present address

†*Department of Mechanical Engineering, Korea Advanced Institute of Science and Technology (KAIST), 291 Daehak-ro, Yuseong-gu, Daejeon 34141, Korea,*

*Corresponding Author: nicola.pugno@unitn.it

Abstract

Insect cuticle has drawn a lot of attention from engineers because of its multifunctional role in the life of insects. Some of these cuticles have an optimal combination of light weight and good mechanical properties, and have inspired the design of composites with novel microstructures. Among these, beetle elytra have been explored extensively for their multilayered structure, multifunctional roles, and mechanical properties. In this study, we investigated the bending properties of elytra by simulating their natural loading condition and comparing it with other loading configurations. Further, we examined the properties of its constitutive bulk layers to understand the contribution of each one to the overall mechanical behavior. Our results showed that elytra are graded, multilayered composite structures that perform better in natural loading direction in terms of both flexural modulus and strength which is likely an adaptation to withstand loads encountered in the habitat. Experiments are supported by analytical calculations and Finite Element Method modeling, which highlighted the additional role of the relatively stiff external exocuticle and of the flexible thin bottom layer, in enhancing flexural mechanical properties. Such studies contribute to the knowledge of the mechanical behavior of this natural composite material and to the development of novel bioinspired multifunctional composites and for optimized armors.

1. Background

Insect cuticle is a biological structure that has been widely investigated for its microstructure because of its crucial role in providing protection and simultaneously permitting locomotion. The composite nature and complex structural design of cuticle determine its mechanical response in terms of strength, bending stiffness, toughness, and wear resistance [1]. Insect cuticles are natural fiber layered composites primarily made of chitin microfibrils and protein, with layers of varying thickness and fiber alignment [2]. The variation in cuticle properties across species is achieved by changing composition, fiber density and orientation, and crosslinking of the protein matrix [3]. Insect cuticle comprises of three layers and the outermost epicuticle is a thin wax layer [4]. The other two layers comprise of chitin micro-fibrils embedded in a protein matrix. One of them is the exocuticle which is hardened by sclerotization process [5], and the other is the unsclerotized endocuticle that is tougher and more flexible [6]. Recent studies have reported on how multi-scale elastic gradients in cuticle-based organs like spider fangs enhance their biomechanical functionality [7]. Such structural gradients were also observed in the tarsal setae of Seven-spot ladybird (*Coccinella septempunctata)*, which enable contact formation with substrates on which they walk and prevents condensation, resulting in increased pad attachment [8].

Elytra are a variation of beetle cuticle with a dorsal layer and a ventral layer, which are connected by a haemolymph space and the columnar trabecular structures [9]. The mechanical interaction between various bulk layers and the constitutive sub-layers together determines the structural performance of the whole elytra. Also, the progressive fiber arrangement in each sub layer of elytra has been shown to be crucial to its mechanical performance [9], while the presence of trabecular structures was hypothesized for energy absorbing function [10]. Elytra have drawn a lot of attention because of their light weight in combination with excellent Young's modulus and hardness, and their peculiar surface texturing resulting in specific optical properties and hydrophobicity [11,12]. Such studies led to the biomimetic design of layered composites with specialized microstructures [10,13,14]. Elytra play an important role in the survival of some beetles by shielding the insect from damage during battles. In addition, the elytron and the flexible wing interaction during flapping has been claimed to improve the aerodynamic force enough to compensate for the weight of the beetle during forward flight [15]. Thus, flexibility of the elytra also plays a role in dynamic interaction with the wind flow during the flight. Studies based on elytra design led to the development of a structural models [10], novel biomimetic composites [14] and were also employed in building construction [16].

In this study, we chose male stag beetles (*Lucanus cervus*) because of their large size and their battle behavior using large puncturing mandibles. Earlier studies on stag beetles were focused on determining bite forces of the mandible and modeling the bites during fights to understand the biomechanical aspects of their mandible movement and its properties [17]. In some instances, the elytra comes in contact with the mandible during battle and the elytra's bending response plays a crucial role in preventing damage. In principle, the elytra of beetles should be resistant to fracture and be rigid enough to sustain bending loads without damage to help in the beetle's survival. Overall, elytra play a multifunctional role in resisting wear from outside environment and protecting the fragile wings when they are folded. Most earlier studies dealing with elytra characterization primarily focused on tensile testing, on dynamic mechanical analysis and, in some cases, on nanoindentation [18–20]. Very few studies have explored the more physiologically relevant bending properties of elytra, which closely simulate natural loading scenario that a beetle experiences in its habitat. Thus, elytron with its multilayered complex microstructure requires a more detailed investigation of its multifunctional mechanical performance. The goal of our study is to provide comprehensive structural and mechanical characterization of the composite elytra in physiological deformation modes and also to investigate the contribution of each layer. Initially, tensile tests were performed on two sample sizes to examine the size effects in the elytra mechanical strength, followed by bending experiments. We then performed tensile tests on each layer to determine their material constitutive properties and to quantitatively assess their contribution to the overall mechanical behavior. The determined layer properties were used to carry out analytical predictions of the overall bending behavior of elytra and also as input for finite element method (FEM) simulation to better understand the deformation mechanisms, delamination and fracture behavior of the multilayer composite structure. The understanding of the role of different layers with different mechanical properties and of the overall elytra structure in its deformation and fracture behavior will help in more detailed design of bioinspired lightweight composites and structures, e.g for impact resistance in advanced applications.

2. Materials and Methods

2.1. Optical and Electron microscopy

The male stag beetles specimens were acquired in dehydrated state from the collection of the MUSE Science Museum of Trento (Trento, Italy). Images of insects were captured using a camera (Sony HDR XR500) as shown in Figure 1A. SEM imaging was performed directly on samples without any preparation because of the relative dryness of elytra samples. Prepared elytra sections from the dissection and mechanical tests were carefully mounted on double-sided carbon tape, stuck on an aluminum stub followed by sputter coating (Manual Sputter Coater, AGAR SCIENTIFIC) with gold. Imaging was carried out using an SEM (EVO 40 XVP, ZEISS, Germany) with accelerating voltages between 5 and 10 kV. *ImageJ* software was used for all dimensional quantification reported in this study [21].

2.2. Mechanical testing

Mechanical tests were performed on the sample sections (Figure 1B), using a Messphysik MIDI 10 (MESSPHYSIK, Germany) Universal Testing Machine and forces were obtained using transducers of two ranges (LEANE Corp., ±10N and METTLER TOLEDO., ±200N). In monotonic tension, specimens were tested in displacement control mode at a rate of 0.01 mm/s. Engineering stresses were calculated as ratio of applied load to the nominal specimen cross sectional area. Axial strains were defined as ratio of change in displacement to initial specimen length. Tensile tests were performed on two sets of samples (three samples from mid location of elytra of each beetle as shown in Figure 1B) with different sizes, large size samples (length= 6.59±1.8 mm, width = 2.62±0.6 mm) and small size samples (length= 1.79±0.26 mm, width = 0.98±0.23 mm).

Bending experiments were performed using the same machine with a custom built 3-point bending setup machined out of hard plastic material on which blunted blades are mounted to achieve line contact during loading. The rate of testing in 3-point bending tests was 0.01 mm/sec. In order to observe and ensure the tests were done without any significant slipping of the sample during tests, all the mechanical tests were monitored using a video camera (Sony HDR XR500) with an objective lens (Olympus 1.5XPF) kept at a distance of ~5 cm from the samples. First set of bending tests (4 samples in each direction, from 4 beetles) on elytra were performed from the hinge location to examine in-plane anisotropy at a given location in the longitudinal and transverse directions orthogonal to each other, as shown in Figure 1B. We then performed a second set of bending tests using samples from middle region of elytra to compare the response of elytra to opposite bending directions (3 samples each from 4 beetles). In this study, the combined epicuticle and exocuticle layers, is referred to as the top layer, the endocutilce referred to as middle layer, and the lower lamination, referred to as bottom layer, is the thinnest of all layers (Figure 1C). The endocutilce primarily constitutes of stacked sub-layers (Figure 1D) and the fiber orientation changes from layer to layer (Figure 1E). Constitutive bulk layers were separated using various procedures (Figure 1F). Top layer was separated by mechanically peeling the bottom layer and carefully scraping the middle layer using a scalpel blade. The bulk middle layer was isolated after soaking the elytra with bottom layer removed, in 10% NaOH solution for 4 hours that enabled easy removal of the top layer. The bottom layer was carefully peeled off from the whole elytron after soaking in water overnight. All the layers were allowed to dry for 24 hours before testing to minimize the hydration effects during the separation processes. Tensile tests (2 samples each from 4 beetles) and bending tests (3 samples each from 4 beetles) on bulk layers were performed on the sections cut from the middle region of elytra as shown in Figure 1B. Sub layers of the middle layer were also separated one by one after soaking the elytra in 10% NaOH for two days, which was proven to dissolve the protein matrix to an extent making the separation easy (Figure 1G).

For this study, 'natural' loading condition was defined as the scenario in which the elytra would be subjected to forces on the outermost epicuticular layer, either by the mandible of an opponent beetle during a fight or at the time of impact due to fall from a tree on the dorsal side (Figure 2A). 'Unnatural loading condition' was defined as elytra being subjected to hypothetical loads from inside by the abdomen expansion, which is unlikely (Figure 2B). The words "natural" and "unnatural" have been adopted to make the distinction of specifying the loading direction. The flexural stress (σ) and strain (ε) from bending experiments were calculated using the following equations from the theory of beams, respectively:

$$\sigma = \frac{3Fl}{2wt^2} \tag{1a}$$

$$\varepsilon = \frac{6\delta t}{l^2} \tag{1b}$$

Where, F is the applied bending force and δ is deflection at the mid-span from the measurements and, w is the beam width, l is the span and t is the thickness. The above calculations were made assuming that the multilayer is homogenous and thus that the maximum stress values occurs at the bottom and top chords of the cross section.

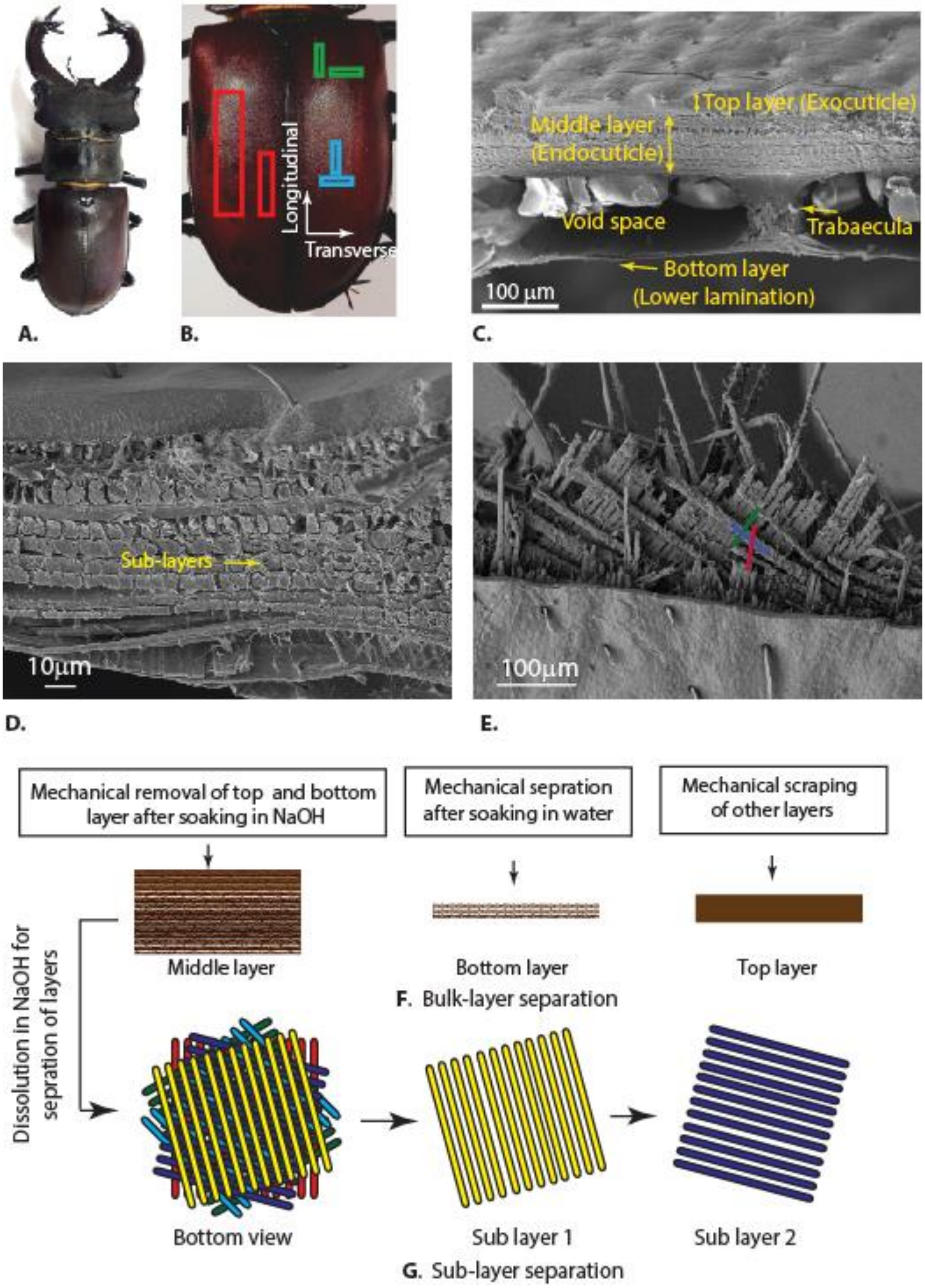

Figure 1. Sample preparation for mechanical testing **A)** image of the stag beetle species used in the study **B)** details of representative size and location of extracted samples (Red = tension samples, green = samples used for in plane anisotropy, blue = samples used for testing asymmery in out of plane direction, **C)** SEM image of whole elytra cross-section showing the constitutive bulk layers, void space and trabecular structures. **D)** SEM image of the elytra cross-section showing the endocuticle constitutive sub-layers. **E**) SEM image of the fractured

elytra showing the macro-fibril orientation in endocuticle **F**) Schematic representation of procedures used for separation of bulk layers and **G**) final separation of sub layers from the middle layer.

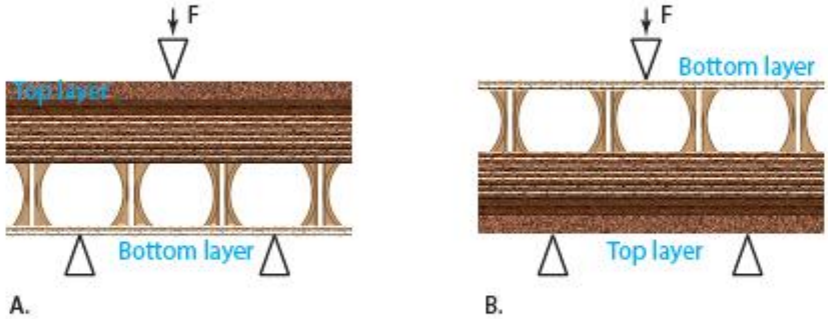

Figure 2. Shematic of the **A**) Three point bending configuration used for testing the natural loading condition response of elytra. **B**) Three point configuration used for testing the bending response in the opposite direction, i.e. unnatural loading.

Analytical modeling

The global tensile properties, i.e. stiffness and strength, of the multilayer system obtained from experiments were verified by a simple rule of mixtures taking into account the contribution of each layer, assuming perfect bonding between them:

$$E_{\text{elytra}} = \sum_{i=1}^{n} f_i E_i \qquad \text{(2a)}$$

$$\sigma_{\text{elytra}} = \sum_{i=1}^{n} f_i \sigma_i \qquad \text{(2b)}$$

where f_i is the volume fraction of each layer, that is the ratio of their thickness over the overall thickness. The derivation of bending properties for a multilayer beam is described in the following [22]. Assuming all material laws as linear elastic and isotropic, a homogenization factor $E_i(y)/E_r$, defined as the ratio of elastic modulus of each material layer to an arbitrary reference modulus E_r, is used to determine the homogenized cross section geometrical properties. The stress distribution along the thickness coordinate y of a beam subjected to axial load N and bending moment M can be evaluated according to the classical Navier's formula, under the hypothesis of planar deformation of bent sections:

$$\sigma = \frac{E(y)}{E_r}\left(\frac{N}{A^*} + \frac{M}{I^*}(y - \overline{y})\right) \tag{3}$$

where $y - \bar{y}$ is the current coordinate with respect to the level of elastic centroid $\bar{y}$, A^* is the homogenized cross-section area defined as:

$$A^* = \int_A \frac{E(y)}{E_r}\mathrm{d}A \tag{4}$$

and I^* is the beam moment of inertia with respect to the beam elastic centroid $\bar{y}$:

$$I^* = \int_A \frac{E(y)}{E_r}(y - \bar{y})^2\mathrm{d}A = \int_{y_i}^{y_e} \frac{E(y)}{E_r}(y - \bar{y})^2 w\mathrm{d}y \tag{5}$$

where w is the beam section width, y_i, y_e are the coordinates of the bottom and top chords of the beam, respectively, with respect to the position of the elastic centroid $\bar{y}$ which can be calculated by the following expression:

$$\bar{y} = \frac{\sum_{i=1}^{n} \frac{E_i}{E_r} w t_i y_{G,i}}{\sum_{i=1}^{n} \frac{E_i}{E_r} w t_i} \tag{6}$$

where E_i, t_i are the Young's moduli and thicknesses of each layer, respectively, and $y_{G,i}$ is the coordinate of the centroid of each layer with respect to an arbitrary reference origin. Eq. (6) is obtained by posing the beam homogenized static moment equal to zero:

$$S^* = \int_A \frac{E(y)}{E_r}(y - \overline{y})dA = 0 \tag{7}$$

Finally, the flexural modulus of the whole elytra can be calculated as:

$$E_f = 12\frac{E_r I^*}{wt^3} \tag{8}$$

where t is the total height of the beam. Finally, in accordance to the three-point bending scheme the maximum transversal force at failure is:

$$F_{max} = \frac{4}{l}\frac{\sigma_f(y) I^*}{y_{i,e}} \tag{9}$$

which is obtained by imposing that the maximum bending moment that the beam is able to carry under the three point bending scheme ($M_{max} = F_{max} l/4$, at the midspan section) is reached when the current flexural stress (Eq. 1a) reaches the failure strength of the corresponding materials σ_f at the bottom or top chords of the beam (y_i and y_e coordinates respectively).

2.3. Computation modeling

A FEM model was developed to simulate three point bending tests and elucidate the deformation/failure mechanism in the elytra. The multilayer was modelled assuming that the constitutive materials of the layers follow a linear elastic and isotropic law, having the same behavior in tension and in compression, as assumed in the analytical model. The average tensile mechanical and geometrical properties of each layer determined from the experimental tests, i.e., elastic modulus, failure strength and strain, and thickness were used as input for simulations. Two cylindrical rigid bars are used to support the elytra beam and a third one at the midspan moves from the top under displacement control (same rate as experiments) in order to apply deflection. The simulated sample has the same dimension of the experiments. Details of the geometry can be found in the Supplementary Information (Figure S2-S3). The top layer and trabecular structures were modelled with under-integrated solid elements with hourglass (spurious deformation modes) controlled. Middle layer and bottom layer are modelled with strain reduced integrated thick shell elements. These elements are specifically suitable for low thickness layers because they have the same degrees of freedom of a shell element but a physical thickness in place of a mathematical one. This allows a better treatment of contact, especially when the plies are subjected to out of plane compressive loading, such as in our experiments. The details of the contact model are explained in supplementary material (Finite Element Modeling details).

The FEM model to study the cushioning effect replaces the two rigid supports with a continuous elastic substrate, composed of two layers simulating the wing and the body of the animal. The mechanical properties of the body were assumed to be the same as that of the top layer of the elytra, since the abdominal external cuticle has similar multilayer structure. The single layer of wing has thickness of 4.4 µm and an elastic modulus E = 3 GPa [23]. The load application follows the same procedure described for the three point bending setup.

3. Results and discussion

3.1. Microstructure of elytra

Microstructural examination showed that elytra are multi-layered composites primarily comprised of three bulk layers of different thickness. The exocuticle is just below epicuticle that is exposed to the environment and the middle bulk layer is comprised of sub layers including microfibers (Figure 3A). The tanned exocuticle consists of chitin micro-fibrils embedded helicoidally in a sclerotized protein matrix [24]. Fiber cross-section shape changed from more of a circular section to that of a square section from top to the bottom, along with reduction in the layer thickness (Figure 3A). The fiber orientation in endocuticle gradually changes from the top sub-layer to the bottom sub-layer (Figure 3B). This is in agreement with observation made in Japanese rhinoceros beetles, *Allomyrina dichotoma* [25]. The ventral layer referred to as bottom layer also has similar structure to that of endocuticle but with thinner sub-layers (Figure 3C). These fibers are bundles made up of thin chitin nano-fibers cross-linked with protein matrix (Figure 3D). Thickness of each bulk layer was quantified for use in our theoretical and numerical modeling. The top layer has a thickness of 45±4 μm and major contribution to the elytra thickness comes from the middle layer, with a thickness of 67±5 μm. Elytra cross section obtained by fracturing showed a change in orientation of fibers between each layer (Figure 3B) and such microstructural organization with changing fiber orientation in consecutive sub-layers is referred to as the Boulingand structure and has been observed in elytra of other beetles [9], crab exoskeletons [26] and also in scales of fish dermal armors [27]. The change in angle of fiber alignment between consecutive sub-layers in the middle layer is of about 78°. The bottom layer is the thinnest of all layers with a thickness of 8±4 μm (Figure 3C). Each fiber bundle was found to have constitutive nanofibers (Figure 3D). We also observed interconnections between fiber bundles in a single sub-layer that are crucial for inter fiber bundle bonding (Figure 3E). These interconnections also enhances the inter-laminar shear strength [28]. The microstructure of a single separated sub-layer showed the interconnections projecting out of plane that might play an important role in the overall mechanics (Figure 3F). Trabecular structures are pillar like connections between the bottom layer and middle layer that are placed in rows along with pore canals (Figure 4A). These trabecular structures have tapered cylindrical shape with higher diameter at the bottom and the top, when compared to the middle (Figure 4B). The empty space between the bottom layer and the middle layer is the void space created by the loss of haemolymph after resorption [29]. After mechanically removing three sub-layers from the middle layer, trabecular shows a reduced diameter (Figure 4C) and its fractured structure show the spiral winding of the layers around the core (Figure 4D). The observed interconnections (Figure 3F) are similar to the ribbon shaped pore canal tubules in crab exoskeletons that were hypothesized to function as a ductile component connecting the fiber bundles to improve the toughness in the thickness direction [26]. In the mineralized shell of Windowpane oyster *(Placuna placenta)*, a different type of screw dislocation like connection centers was observed to enhance the interface toughness by reducing the delamination [30].

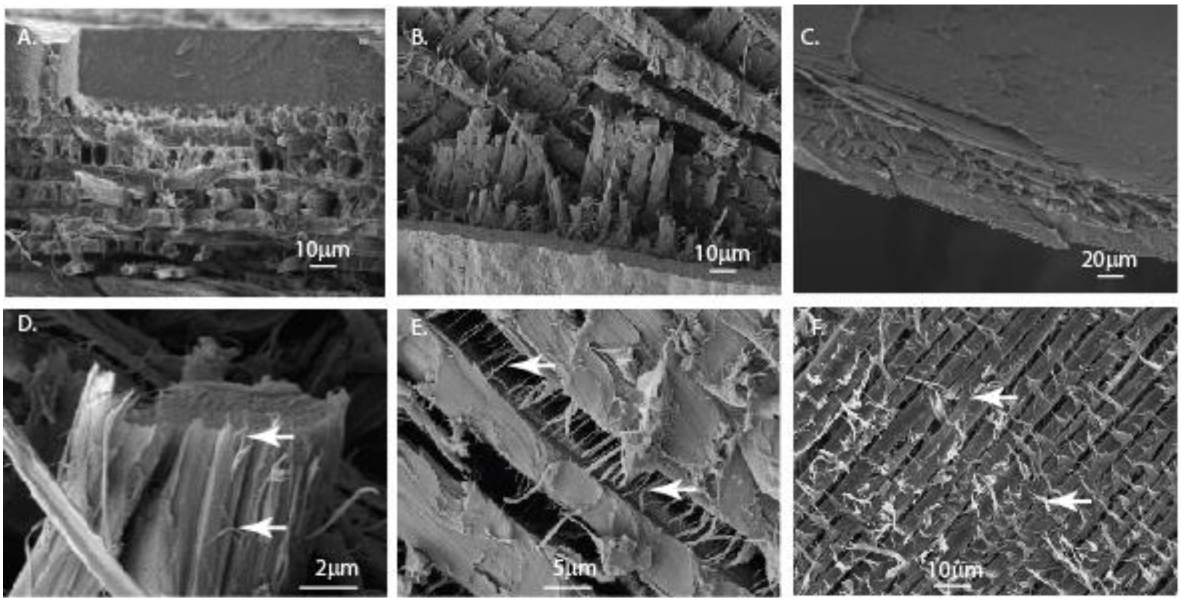

Figure 3. SEM images showing the microstructure of elytra **A**) Fractured cross-section showing the exocuticle with relatively smooth surface and the endocutilce with change in fiber diameter and layer thickness from top to bottom sublayers. **B**) Top view of fractured surface of elytra show fiber rotation in sublayers. **C**) Lower lamination made by a composite layer with sub-layers made of relatively smaller fiber cross-section section. **D**) Fractured fiber bundle showing its constitutive nanofibers (arrows), **E)** interconnections (arrows) between fiber bundles in a layer, and **F**) a single separated sub-layer shows the broken fibrillar connections (arrows) between two adjacent sub- layers.

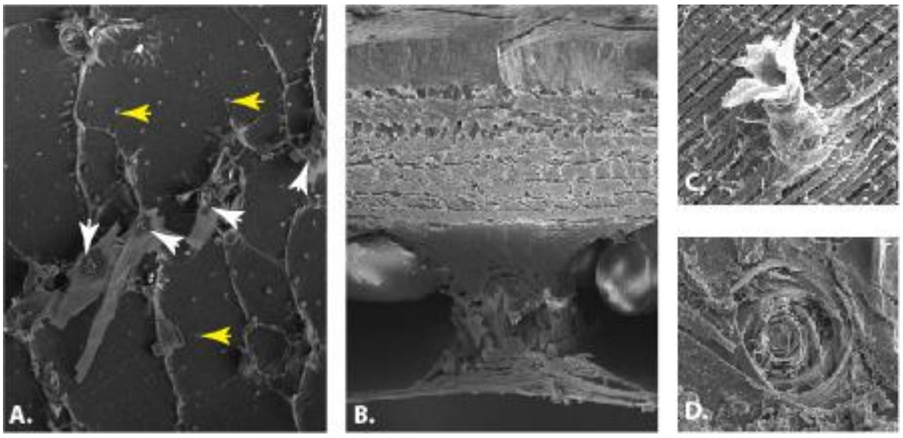

Figure 4. Elytra microstructure. **A)** Large scanned area showing distribution pattern trabecular structures of elytra (white arrows) and pore canals (yellow arrows). **B)** Cross-section showing how trabecular connects the middle layer and bottom layer. **C)** Trabecular structure showing inner structure after peeling of three layers as shown in experimental

section. **D)** Top cross-sectional view of a trabecular structure showing concentric layers and their spiral woven structure.

3.2. Mechanical testing and modeling

3.2.1. Tensile strength and Young's modulus of the elytra

Stress-strain curves from these experiments showed repeatability in terms of a sudden drop in load that is representative of a brittle like fracture of the cuticle (Figure 5A-B). In large samples, the average values of fracture strength and modulus of elytra were 65.0±25.5 MPa and 1.9±0.6 GPa, as reported in Table 1. In case of small size samples, the average values of fracture strength and modulus of elytra were 81.7±35.1 MPa and 1.29±0.5 GPa, as shown in Table 1. This sample size dependent variation can be attributed to the presence of trabecular structures and pore canals acting as defects. So, the density and distribution of these structures could be a significant factor. If we consider the surface area of the samples, the larger samples have an average surface area of 17.3 mm^2 and the smaller samples have an average surface area of 1.75 mm^2. We investigated the scaling effects in tensile testing of the specimens. Using Weibull's (weakest link) theory we expect:

$$\frac{\sigma_1}{\sigma_2} = \left(\frac{V_2}{V_1}\right)^{\frac{1}{m}} \tag{10}$$

where, σ and V, are the tensile strength and volume of the specimens. The estimated value of the Weibull's modulus *m* is 10.25. Similarly, according to an energy dissipation on a fractal volume of dimension *D* [31] we expected:

$$\frac{\sigma_1}{\sigma_2} = \left(\frac{V_1}{V_2}\right)^{\frac{D-3}{6}} \tag{11}$$

The estimated value of *D* is 2.41 confirming a fractal domain intermediate between a Euclidean surface (*D*=2) and a volume (*D*=3). Our whole elytra experimental results were comparable to that of other beetle species [17], in particular Hercules beetle (*Dynastes hercules*) with modulus and strength values of 3.1-14 GPa and 26.8-62.9 GPa [32]. The large variability observed in fracture strength could be attributed to the biological variation, density and distribution of observable defects such as pore canals and trabecular structures, and in addition the effects introduced from the sample preparation. During sample preparation, it is difficult to create samples which are identical in terms of distribution and density of trabecular structures and also the pore canals. In addition, the location of these structures has a significant effect depending on whether the cut was made through them or close to them. In such cases, these defects could possibly act as cracks and notches if they are on the edges of the sample (along the length) and close to the stress concentration regions, and result in significant reduction of fracture strength. In contrast, if these structures are not present on the edges, the sample could result in higher fracture strength. Such variations were also observed in the tanned elytra of *Tribolium castaneum* [33]. To understand the detailed contribution of various bulk layers, we have performed tensile tests on separated layers. The top layer has a nearly linear stress-strain response and failed suddenly with the load dropping to zero (Figure 5C). Middle layer also displayed a linear stress-strain response but towards the end showed a slight drop in load corresponding to initiation of fiber delamination followed by a sudden failure (Figure 5D). Bottom layer also displayed a linear stress-strain response and load dropped to zero with sudden failure (Figure 5E). The top layer has a Young's modulus of 4.14±0.46 GPa and a fracture strength of 203.5±62.2 MPa. Whereas, the middle layer has a modulus of 2.73±0.77 GPa and fracture strength of 124.5±37.4 MPa. The bottom layer has a modulus of 2.62±0.92 GPa and fracture strength of 101.6±46.6 MPa. Thus, top layer has stiffer response and also higher failure strength, as compared to other bulk layers. Using the measured mechanical properties of single layers, by a classical rule of mixture (Equations 2a-b, see Materials and methods section), we estimated Young's modulus and tensile strength of multilayer to be 2.1 GPa and 85.8 MPa, respectively. These estimates are comparable with the experimentally measured whole elytra values.

It emerges that tensile strength gradually decreases from top layer to bottom layer and stiffness also followed a similar trend which could be an optimization for puncturing resistance. In tension, failure was observed as a brittle fracture propagating in the top hard layer, pull-out and breaking of fibers in the other layers. The observed bridging fibers between adjacent fiber bundles and also between sub-layers aid in increasing the fracture resistance (Figures 3E-F). Overall, the Bouligand (helicoidal) structure of the layers is known to increase the fracture toughness [34,35].

Table 1.Tensile and bending mechanical properties of elytra and its constitutive layers. (in brackets: Standard Mean of Error)

Tensile mechanical properties

Cuticle/layer	Young's Modulus [GPa]	Fracture strength [MPa]
Elytra (large)	1.90±0.6 (0.23)	65.0±25.5 (10.1)
Elytra (small)	1.29±0.5 (0.32)	81.7±35.1 (21.4)
Top layer	4.14±0.46 (0.33)	203.5±62.2 (63.1)
Middle layer	2.73±0.77 (0.19)	124.5±37.4 (25.2)
Bottom layer	2.62±0.92 (0.93)	101.6±46.6 (36.5)

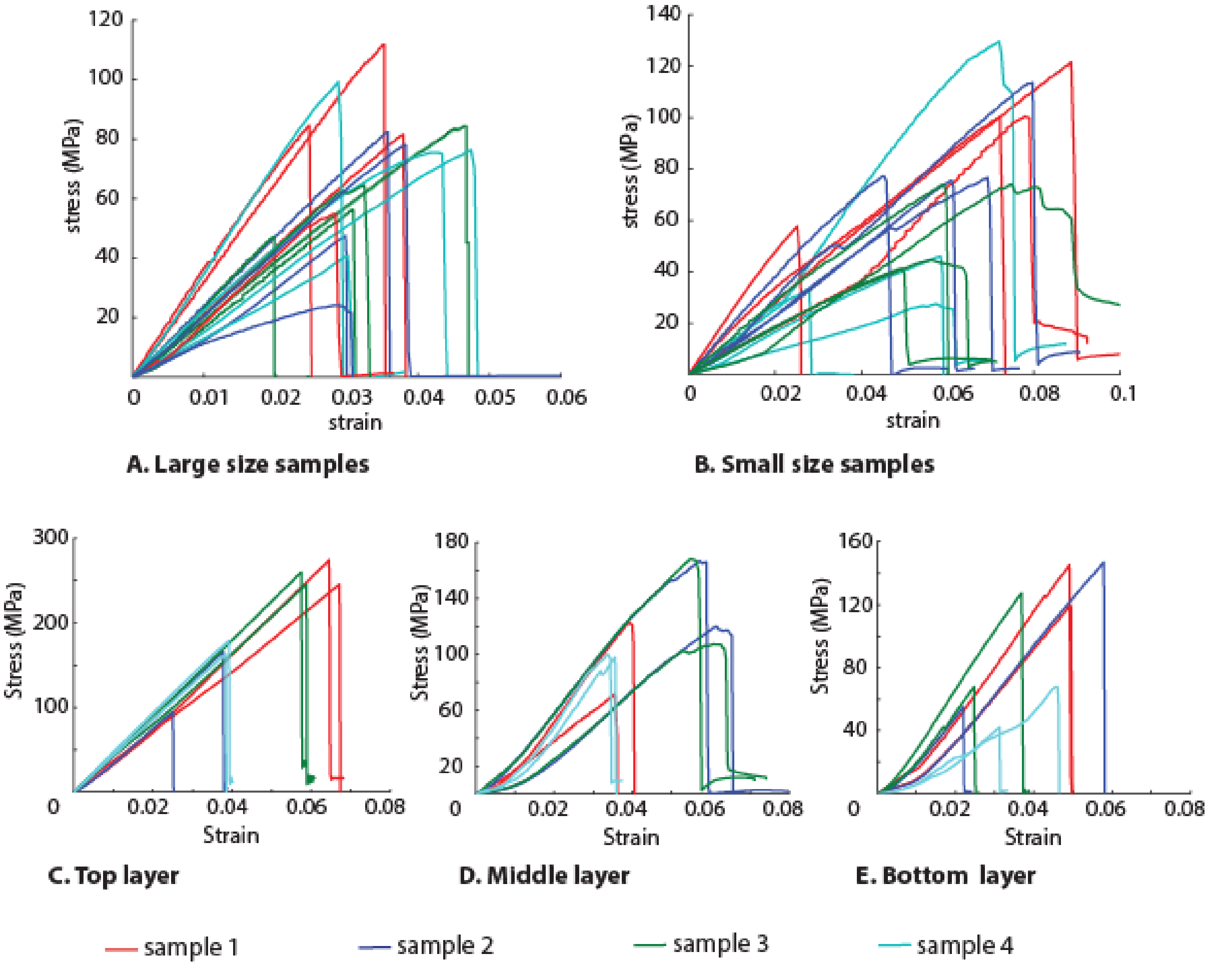

Figure 5. Stress-strain relationships showing mechanical behavior from tension experiments of elytra: **A**) Larger samples showing brittle like fracture and **B**) Smaller size samples showing similar behavior. **C**) Top layer having a linear response with sudden failure and **D**) middle layer also showing linear response with a drop due to initiation of fiber delamination followed by sudden failure, and **E**) bottom layer also showing linear response with a sudden failure.

3.2.2. Flexural modulus and flexural strength of elytra

Experimental flexural stress-strain curves showed a nearly linear response up to failure and the dispersion in the mechanical properties is significant (Figure 6A-B). Flexural strength and flexural modulus were 312±103 MPa and 451±91 MPa, respectively in the longitudinal direction. A similar range of values of flexural strength (333±94 MPa) and flexural modulus (421±59 MPa) was observed in the orthogonal transverse direction. These results demonstrate that there is no significant anisotropy in the bending response of elytra at a given location. To examine dependency of loading condition on bending behavior of elytra, we performed the second set of bending experiments. Stress-strain curves from these experiments were observed to be significantly different (Figure 6C-D). In natural loading condition, some specimens failed suddenly and some failed gradually with progressive damage. In case of unnatural loading condition, step wise load drop was observed with increasing strain after a certain deflection. Flexural strength and flexural modulus in natural loading direction were 222±172 MPa and 811±650 MPa respectively. In unnatural loading direction, the values of flexural strength and flexural modulus were 73±39 MPa and 455±287 MPa respectively, i.e. nearly one half with respect to the real operating scenario (Table 2). Such high variability in modulus and strength for each configuration can be attributed to the inherent biological differences in our extracted beetle samples, regional variation in the elytra and the limited availability because of their endangered status. The variation in properties from hinge location to mid location was in agreement with earlier observations made on 5 species of beetles [36]. Flexural modulus values are lower than that of tensile modulus, and this is also affected by the void space in elytra. In contrast, flexural strength is three times that of the tensile strength. This is a noteworthy observation in elytra mechanics, with a higher mechanical strength in bending as opposed to tension. Such observations were also made in glass fiber reinforced polyamide composite materials [37]. The observed higher bending performance in elytra natural loading condition is similar to the behavior of functional graded ceramic engineering materials [38]. In ceramic based functionally graded materials, the asymmetric bending behavior is achieved by varying the composition of the ceramic components, unlike elytra which are made of brittle and fibrous components.

Stress-strain curves of top layer displayed behavior similar to that of a brittle material and that of the middle layer were similar to a ductile material (Figure 6E-F). Results from these tests showed that the top layer has a flexural strength of 392±178 MPa and flexural modulus of 8.29±4.74 GPa, while the flexural strength and flexural modulus of middle layer were observed to be 221±85 MPa and 3.95±1.45 GPa respectively (Table 2). The exocuticle of elytra of Giant water bugs (*Hydrocyrius columbiae)* was observed to have microfibrils of diameter ~45 A^{o} and center to center distance of ~65 A^{o}, are arranged helicoidally with a rotation of 6 to 7 per plane [39]. These densely packed chitin microfibrils embedded in tanned protein matrix might act as reinforcements and the helicoidal arrangement results in isotropic and enhanced stiffness of the exocuticle. Such improvement in mechanical properties due to the presence of the helicoidal fiber arrangement has been proved by testing bioinspired laminate composites [40]. Flexural modulus of these layers was an order of magnitude higher and flexural strength was of the same order, as compared to the whole elytra. It was not possible to measure flexural properties of the bottom layer using the current experimental set-up, because of its extremely low thickness and bending stiffness, thus, we can neglect.

Table 2. Flexural mechanical properties of elytra and its constitutive layers. (in brackets : Standard Mean of Error)

Table 1. **Bending mechanical properties**

Cuticle/Layer	**Flexural strength [MPa]**	**Flexural Modulus [MPa]**
Natural direction	222±172 (138)	811±650 (420)
Unnatural direction	73±39 (17)	455±287 (135)
Top layer	392±178 (99)	8295±4745 (1543)
Middle layer	221±85 (52)	3952±1452 (612)

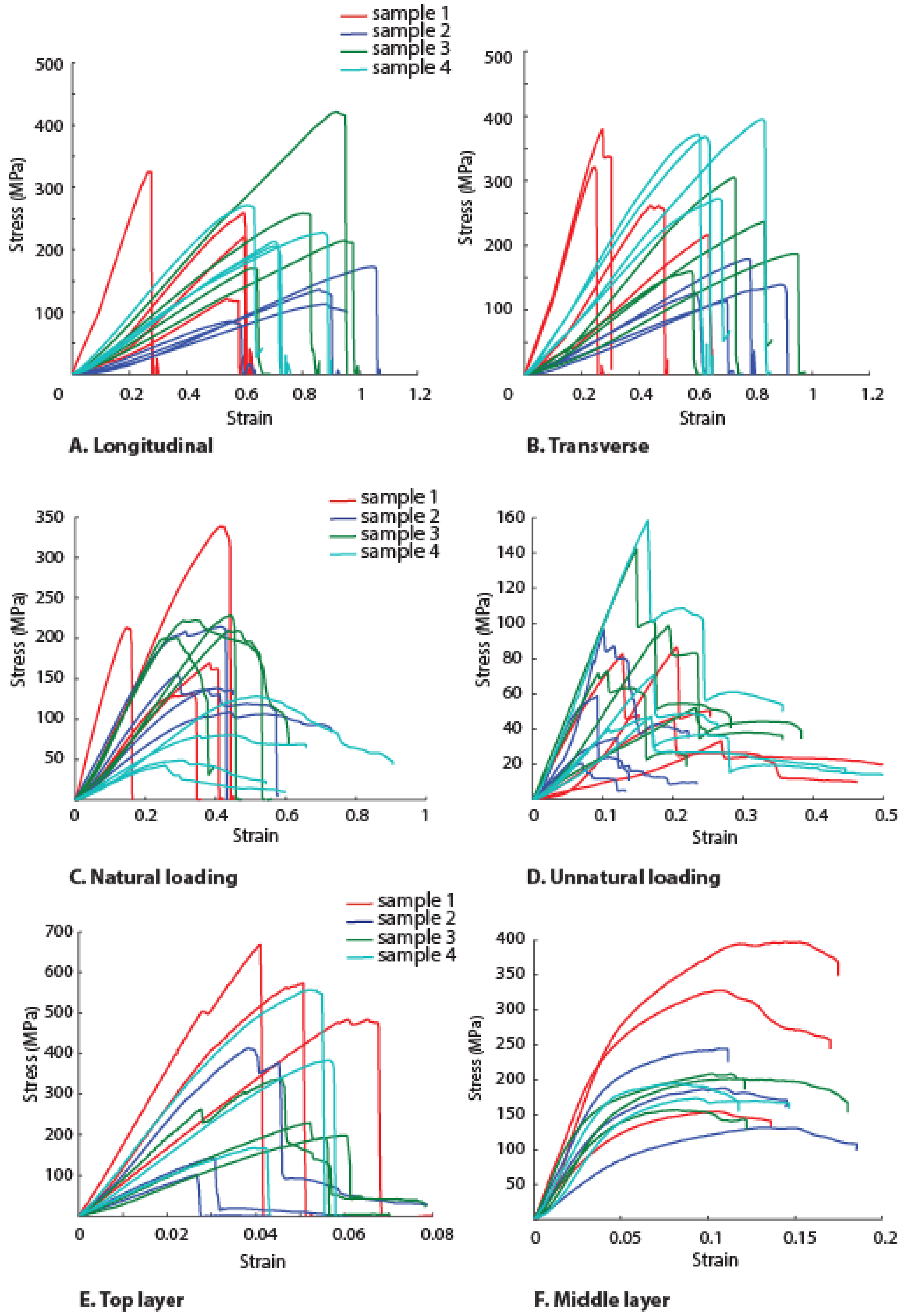

Figure 6. Bending stress strain curves from **A**) longitudinal direction and **B**) transverse direction **C**) natural loading conditions and **D**) unnatural loading condition, **E**) top layer and **F**) middle layer.

The position $\bar{y}$ of the neutral axis is the level at which the bending stresses and strains change sign, is calculated to be ~12 μm below the interface between the top layer and the middle layer, using average values of each layer's elastic modulus and thickness. To analyze the role of trabecular structures, in particular their height, we analyzed the role of the void space between middle layer and bottom layer by varying it in the calculations from 0 to 80 μm. According to Eq. (3), we obtained that this distance of neutral axis ranges from 9 to 13 μm, thus the relative position of the elastic centroid is nearly constant within the endocuticle, suggesting another role for the void space other than optimizing bending properties. On the other hand, the position of neutral axis is significantly affected by the variation in elastic modulus and thickness of each layer, as expected for a composite bilayer. This indicates that the multilayer grading sequence of thickness and elastic moduli is optimized for better mechanical performance in bending. In particular, the elytra multilayer combination is a suitable design for the natural loading conditions, since the position of the elastic centroid confines compression stresses in the top brittle layer and tension in the tough composite middle layer, optimizing the local stress state for the specific constitutive laws of materials. This results in a ratio of 3 between the bending mechanical properties in the two opposite directions (Table 3).

FEM simulations resembling three-point bending tests (Figure 7-8) were performed to closely understand the mechanics of bending deformation and fracture behavior. Results were consistent with experiments predicting the variation in flexural modulus and flexural strength in different loading conditions, despite the approximation of linear elastic isotropic material and same constitutive behavior in tension and compression for each layer. In natural loading condition, an initial load drop (Figure 7, point 2) was observed due to delamination in the middle layer and failure of the bottom layer, which suggests an optimized design between the bottom layer and interlamellar strength. The latter, assumed as a free parameter, was estimated to be about 5.5 MPa, and allowed us to obtain the closest response with respect to the average force displacement bending curve of elytra (see Supplementary Information, Figure S4). The results suggest optimal interface strength ($\tau_{lim} = 5.5$ MPa) in the elytra multilayers. Similar findings were observed in impact simulations based on composite armors [41]. The final drop occurs when the whole elytra fails (Figure 7A). After the first drop (point 2), a recovery of the load with reduced stiffness at point 3 is attributed to the bending resistance from the intact top layer and middle layer. The deformation sequence is shown using snapshots of simulation corresponding to various stages of deformation and complete failure (Figure 7B). In the unnatural loading condition, buckling of bottom layer was observed as it experiences compression and its contribution to flexural modulus and strength becomes nearly negligible (Figure 8A), causing the first drop in the force (point 2). Delamination within the middle layer results in second load drop (Figure 8B, point 3) and a consequent further flexural stiffness reduction. Complete fracture of the whole elytra starts from the failure of the hard layer at the bottom in this configuration (point 4). Thus, failure in this condition initiates from top layer depending on its tensile properties, followed by delamination in the middle layer and final overall collapse. Thus, we claim that the bottom layer is able to play a crucial role only in natural loading bending response. Simulations are in good quantitative agreement with experimental results.

It should be noted that all the experiments were performed on dehydrated specimens because of the near threatened (IUCN Red list) state of the selected species. As described in earlier studies, dehydration may significantly increase the mechanical properties of the cuticle [40]. So the mechanical properties of the whole elytra specimens must be considered in our study as related to the dried samples and as upper-bound of living samples. Also an artificial rehydration cannot be considered representative of the living material, for which in any case the non-symmetric bending properties are also expected as confirmed by the related nonlinear mechanism (buckling of the bottom layer). Moreover, the sub-layers separation methods could have affected their mechanical properties, i.e. by damaging layers and thus reducing the properties as compared to the properties in the native state. However, the numerical and analytical comparisons (which use single layer properties as inputs) with the experimental measurements on the multi-layered elytra suggest a limited damaging during the layer separation process.

According to the experimental and simulation observations we can define two mechanisms in relation to the direction of bending. In natural bending all the layers contribute to bending stiffness whereas in the unnatural bending the bottom layer's contribution can be neglected as it experiences buckling in compression due to its low thickness. Thus in the natural loading case, the total thickness of the multilayer enters into play, while in the unnatural loading case, only the thickness of top layer and the middle layer could be considered. According to Eq. (8) we estimate the flexural moduli in the two loading conditions $E_{f,n}$=1.46 GPa and $E_{f,u}$=0.96 GPa, where the subscripts n and u denote the natural and unnatural loading conditions, respectively. From Eq. (9), in case of natural bending first failure occurs in the bottom layer. After that, the reactive section is composed by just the top layer and middle layer and the overall failure of the multilayer occurs for the rupture in tension of the middle layer. In the unnatural bending case, the maximum force at failure is given by the rupture of top layer at F_u = 1.15 N. Both analytical and simulation results are in good agreement with experimental results. The final plateau region obtained both in FEM simulation and experiments correspond to the friction slipping of the sample at the contact points (Figure 8B). Results from experiments, simulation and analytical calculation are summarized for comparison in Table 3.

In the real situation, the elytra and the folded wing underneath it are continuously supported by the body. The trabecular structures with the void space between them may provide a cushioning effect to further protect the fragile wing and the body from external loads. The supports of the three point bending set up are substituted by a continuous substrate simulating the insect wing and body under the protective elytra. In the Supplementary Figure S5, the distribution of stresses in the wing and the body under the same concentrated load ($F_{n,max}$, previously determined) is depicted. Simulation results showed that elytra structure is subjected to local higher stresses due to the presence of void space inside as compared to the case without it (3.9 MPa vs. 2.9 MPa), since trabecular structure concentrate the load, but performed better in absorbing the energy. Indeed, under the same external load F, the strain energy values in the body were less than one half compared to the elytra model without void space (2.2 µJ vs. 4.92 µJ). This is a good indication that the presence of the void space in elytra helps in mitigating the energy transfer to the body by allowing higher deformation of the top layers and spreading the load over a large area (see Supplementary Figure S5). In some beetles the void space could be filled haemolymph but because we are not sure of its occurrence in the natural state of our study species, we have not considered this complex scenario.

Table 3. Summary and comparison of experimental, analytical and simulation results of elytra mechanical properties.

		Experiments	Analytical	FEM Simulations
Tensile properties	**σ [MPa]**	81.7 ± 35.1	85.8	-
	***E* [GPa]**	1.29 ± 0.32	2.10	-
Bending properties	$E_{f,n}$	0.81 ± 0.42	1.46	0.94

	[GPa]			
	E**f, u [GPa]**	0.46 ± 0.14	0.96	0.83
	σf, n [GPa]	0.22± 0.14	0.14	0.26
	σf,u [GPa]	0.07± 0.04	0.07	0.09
	Fmax,n [N/mm]	2.98±1.82	2.31	3.31
	Fmax,u [N/mm]	1.20±0.64	1.15	1.15

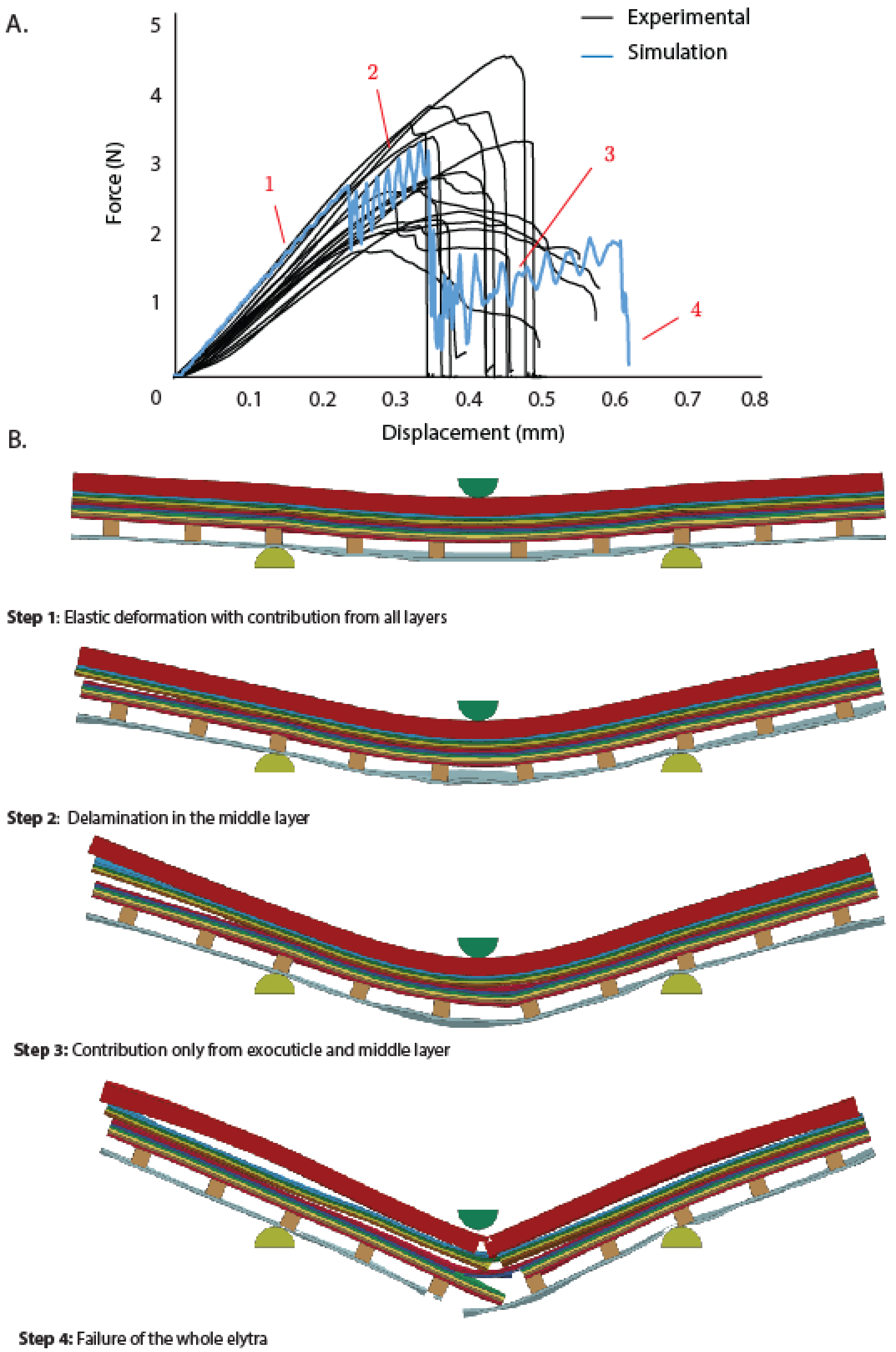

Figure 7. FEM simulation results of bending in natural loading condition **A**) showing the force displacement relationship and, **B**) snapshots showing the corresponding stages of bending.

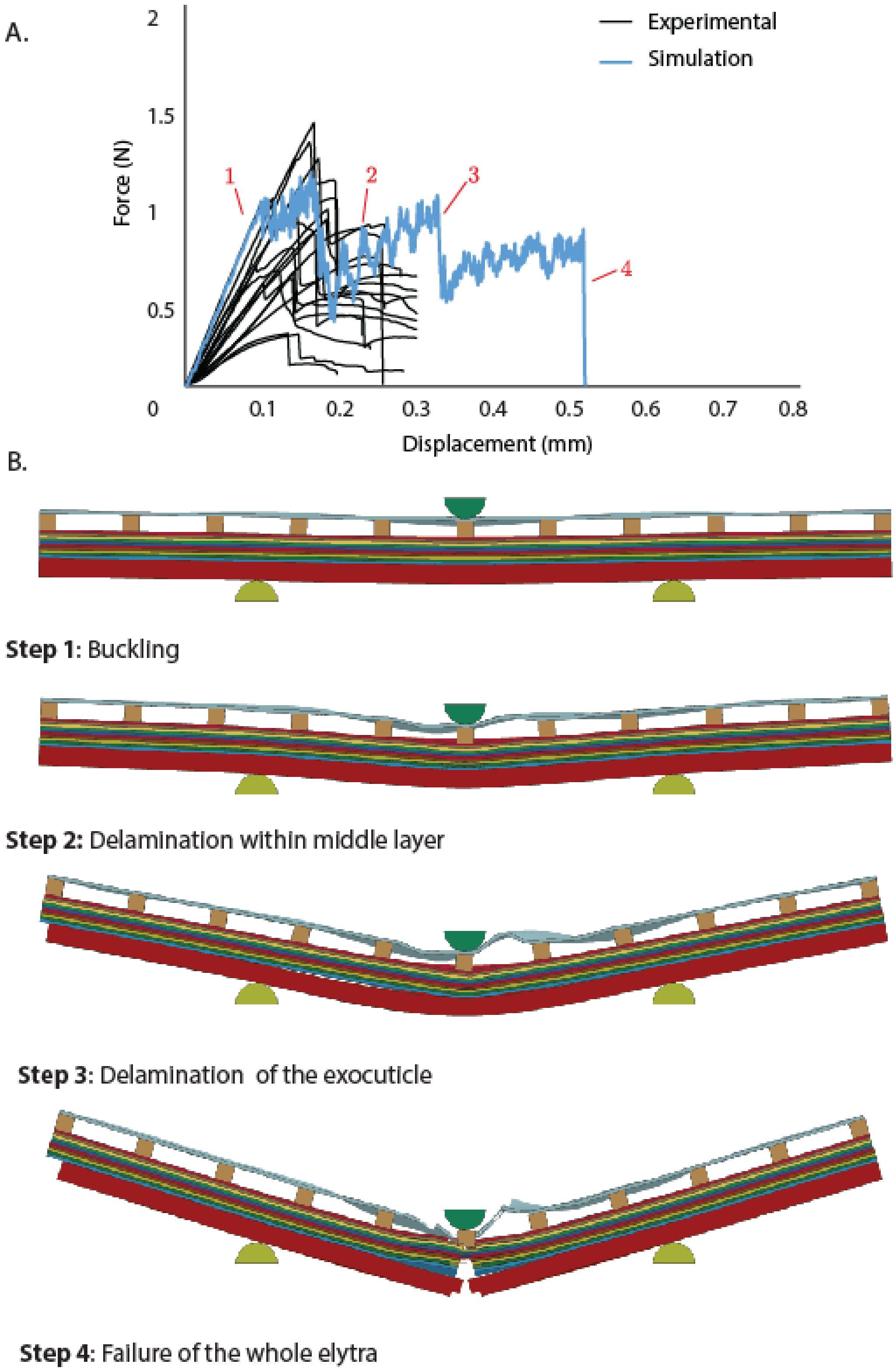

Figure 8. FEM simulation results of bending in unnatural loading condition **A**) showing the force displacement relationship and, **B**) snapshots showing the corresponding stages of bending.

4. Conclusions

Characterization of Stag beetle elytra by means of mechanical experiments and simulations, gave a new insight into the role of microstructure on its mechanical behavior. Particularly, the synergy between materials and structural arrangement by combination of layer stacking results in enhanced stiffness and load bearing capacity upon bending. The combination of hard top layer performing better in compression and the flexible bottom layer that contributes only in tension is optimized to provide higher bending stiffness in close to natural loading condition. Also, the position of flexible bottom layer far away from the centroid of the cross section with the aid of connecting trabecular structures allows the beetle to reduce the cuticle weight by maximizing the moment of inertia, and thus flexural strength and modulus. At the same time this structure provides cushioning capability, reducing the energy transfer to the beetle body and internal organs. FEM models developed in this study have the capability of modeling fracture and large deformations and could be extended to other biological structures similar to elytra or their engineering bio-inspired designs. These results could help in designing structures such as body armors with asymmetric bending properties tuned to perform better in terms of energy absorption and strength in a particular loading condition, with improved ergonomics and flexibility together with external rigidity.

Acknowledgments: NMP is supported by the European Commission H2020 under the Graphene Flagship (WP14 ‘Polymer Composites’, no. 696656) and under the FET Proactive (“Neurofibers” no. 732344), as well as by the Italian Ministry of Education, University and Research (MIUR) under the "Departments of Excellence" grant L.232/2016. N.M.P is also supported by Fondazione Caritro under "Self-Cleaning Glasses" No. 2016.0278, as L.K. SS acknowledges financial support from Ermenegildo Zegna Founder’s Scholarship 2017. The authors thank Nicola Angeli (MUSE, Trento) for the help with SEM imaging.

Author Contributions: LK and NMP designed the study. MM helped in acquiring the samples. HSG contributed in technical discussions and manuscript editing. LK performed the mechanical experiments. SS performed the FEM simulations. LK and SS wrote the first draft of the manuscript (corresponding sections). NMP supervised the study and developed the analytical model. All authors approved the contents of the article.

Conflicts of Interest: The authors declare no conflict of interest.

References

1. Vincent JF V, Wegst UGK. 2004 Design and mechanical properties of insect cuticle. *Arthropod Struct. Dev.* **33**, 187–99. (doi:10.1016/j.asd.2004.05.006)

2. Gunderson S, Schiavone R. 1989 The Insect Exoskeleton : A Natural Structural Composite. *J. Miner. Met. Mater. Soc.* , 60–62.

3. Vincent JFV. 2002 Arthropod cuticle: a natural composite shell system. *Compos. Part A Appl. Sci. Manuf.* **33**, 1311–1315. (doi:10.1016/S1359-835X(02)00167-7)

4. Hadley NF. 1986 The Arthropod cuticle. *Sci. Am.* **255**, 104–112. (doi:10.1038/ scientificamerican 0786-104)

5. Hopkins TL, John Krchma L, Ahmad SA, Kramer KJ. 2000 Pupal cuticle proteins of Manduca sexta: Characterization and profiles during sclerotization. *Insect Biochem. Mol. Biol.* **30**, 19–27. (doi:10.1016/S0965-1748(99)00091-0)

6. Roux-Pertus C, Oliviero E, Viguier V, Fernandez F, Maillot F, Ferry O, Fleutot S, Mano JF, Cleymand F. 2017 Multiscale characterization of the hierarchical structure of Dynastes hercules elytra. *Micron* **101**, 16–24. (doi:10.1016/j.micron.2017.05.001)

7. Bar-On B, Barth FG, Fratzl P, Politi Y. 2014 Multiscale structural gradients enhance the biomechanical functionality of the spider fang. *Nat. Commun.* **5**, 3894. (doi:10.1038/ncomms4894)

8. Peisker H, Michels J, Gorb SN. 2013 Evidence for a material gradient in the adhesive tarsal setae of the ladybird beetle Coccinella septempunctata. *Nat. Commun.* **4**, 1661. (doi:10.1038/ncomms2576)

9. Kamp T Van De, Greven H. 2010 On the architecture of beetle elytra. *Entomol. heute* **22**, 191–204.

10. Guo T, Wang Y-F. 2011 Energy absorbing structures imitating trabecular of beetle cuticles.*Engineering Mech.* **28**, 246–256.

11. Stavenga DG, Wilts BD, Leertouwer HL, Hariyama T. 2011 Polarized iridescence of the multilayered elytra of the Japanese jewel beetle, Chrysochroa fulgidissima. *Philos. Trans. R. Soc. Lond. B. Biol. Sci.* **366**, 709–723. (doi:10.1098/rstb.2010.0197)

12. Onelli OD, Kamp T Van De, Skepper JN, Powell J, Rolo TDS, Baumbach T, Vignolini S. 2017 Development of structural colour in leaf beetles. *Sci. Rep.* **7**, 1–9. (doi:10.1038/s41598-017-01496-8)

13. Dai Z, Zhang Y, Liang X, Sun J. 2008 Coupling between elytra of some beetles: mechanism, forces and effect of surface texture. *Sci. China. C. Life Sci.* **51**, 894–901. (doi:10.1007/s11427-008-0124-7)

14. Chen J, Wu G. 2013 Beetle forewings : Epitome of the optimal design for lightweight composite materials. *Carbohydr. Polym.* **91**, 659–665. (doi:10.1016/j.carbpol.2012.08.061)

15. Le TQ, Truong T Van, Park SH, Truong TQ, Ko JH, Park HC, Byun D. 2013 Improvement of the aerodynamic performance by wing flexibility and elytra – hind wing interaction of a beetle during forward flight. *J.Roc.Soc.Interface.* **55** (DOI: 10.1098/rsif.2013.0312)

16. van de Kamp T, Doerstelmann M, dos Sanots Rolo T, Baumbach T, Menges A, Knippers J. 2015 Beetle Elytra as Role Models for Lightweight Building Construction. *Entomol. heute* **27**, 149–158.

17. Goyens J, Dirckx J, Dierick M, Van Hoorebeke L, Aerts P. 2014 Biomechanical determinants of bite force dimorphism in Cyclommatus metallifer stag beetles. *J. Exp. Biol.* **217**, 1065–71. (doi:10.1242/jeb.091744)

18. Lomakin J, Arakane Y, Kramer KJ, Beeman RW, Kanost MR, Gehrke SH. 2010 Mechanical properties of elytra from Tribolium castaneum wild-type and body color mutant strains. *J. Insect Physiol.* **56**, 1901–6. (doi:10.1016/j.jinsphys.2010.08.012)

19. Sun J, Tong J, Zhang Z. 2009 Nanomechanical Properties and the Hierarchical Structure of Elytra Cuticle of Dung Beetle (Copris ochus Motschulsky). *International*

Conference on Mechatronics and Automation, 4277–4282.

20. Sun J, Tong J, Chen DH, Lin J, Liu X, Wang Y. 2016 Micro-tensile Testing of the Lightweight Laminated Structures of Beetle Elytra Cuticle Micro-tensile *The 3rd International Conference of Bionic Engineering*,**7**(1),6-12.

21. Abràmoff MD, Magalhães PJ. 2004 Image Processing with ImageJ. *Biophotonics Int.*

22. Timoshenko S, Goodier J. 1970 *Thoery of Elasticity*. Third edition.

23. Ha NS, Jin TL, Goo NS, Park HC. 2011 Anisotropy and non-homogeneity of an Allomyrina Dichotoma beetle hind wing membrane. *Bioinspir. Biomim.* **6**, 46003. (doi:10.1088/1748-3182/6/4/046003)

24. van de Kamp T, Riedel A, Greven H. 2016 Micromorphology of the elytral cuticle of beetles, with an emphasis on weevils (Coleoptera: Curculionoidea). *Arthropod Struct. Dev.* **45**, 14–22. (doi:10.1016/j.asd.2015.10.002)

25. Chen J, Dai G, Xu Y, Iwamoto M. 2007 Optimal composite structures in the forewings of beetles. *Compos. Struct.* **81**, 432–437. (doi:10.1016/j.compstruct.2006.09.006)

26. Chen P-Y, Lin AY-M, McKittrick J, Meyers MA. 2008 Structure and mechanical properties of crab exoskeletons. *Acta Biomater.* **4**, 587–96. (doi:10.1016/j.actbio.2007.12.010)

27. Zimmermann EA, Gludovatz B, Schaible E, Dave NKN, Yang W, Meyers MA, Ritchie RO. 2013 Mechanical adaptability of the Bouligand-type structure in natural dermal armour. *Nat. Commun.* **4**, 2634. (doi:10.1038/ncomms3634)

28. Ribbans B, Li Y, Tan T. 2016 A bioinspired study on the interlaminar shear resistance of helicoidal fiber structures. *J. Mech. Behav. Biomed. Mater.* **56**, 57–67. (doi:10.1016/j.jmbbm.2015.11.004)

29. Arakane Y, Lomakin J, Gehrke SH, Hiromasa Y, Tomich JM, Muthukrishnan S, Beeman RW, Kramer KJ, Kanost MR. 2012 Formation of rigid, non-flight forewings (elytra) of a beetle requires two major cuticular proteins. *PLoS Genet.* **8**, e1002682. (doi:10.1371/journal.pgen.1002682)

30. Li L, Ortiz C. 2015 A natural 3D interconnected laminated composite with enhanced

damage resistance. *Adv. Funct. Mater.* , 3463–3471. (doi:10.1002/adfm.201500380)

31. Carpinteri A, Pugno N. 2005 Are scaling laws on strength of solids related to mechanics or to geometry? *Nat. Mater.* **4**, 421–423. (doi:10.1038/nmat1408)

32. Conrad MB. 2014 Bioinspired composites design : mechanical and optical characterization of the Hercules beetle elytra. Master's thesis, Naval Post-Graduate School, California, United States of America.

33. Lomakin J, Huber P a, Eichler C, Arakane Y, Kramer KJ, Beeman RW, Kanost MR, Gehrke SH. 2011 Mechanical properties of the beetle elytron, a biological composite material. *Biomacromolecules* **12**, 321–35. (doi:10.1021/bm1009156)

34. Chen B, Peng X, Cai C, Niu H, Wu X. 2006 Helicoidal microstructure of Scarabaei cuticle and biomimetic research. *Mater. Sci. Eng. A* **423**, 237–242. (doi:10.1016/j.msea.2005.11.069)

35. Suksangpanya N, Yaraghi NA, Kisailus D, Zavattieri P. 2017 Twisting cracks in Bouligand structures. *J. Mech. Behav. Biomed. Mater.* , 1–20. (doi:10.1016/j.jmbbm.2017.06.010)

36. Yu M, Hermann I, Dai Z, Gitis N. 2013 Mechanical and Frictional Properties of the Elytra of Five Species of Beetles. *J. Bionic Eng.* **10**, 77–83. (doi:10.1016/S1672-6529(13)60201-2)

37. Thomason JL. 2008 The influence of fibre length, diameter and concentration on the strength and strain to failure of glass fibre-reinforced polyamide 6,6. *Compos. Part A Appl. Sci. Manuf.* **39**, 1618–1624. (doi:10.1016/j.compositesa.2008.07.002)

38. Tsukada G, Sueyoshi H, Kamibayashi H, Tokuda M, Torii M. 2014 Bending strength of zirconia/porcelain functionally graded materials prepared using spark plasma sintering. *J. Dent.* **42**, 1569–1576. (doi:10.1016/j.jdent.2014.09.012)

39. Zelazny B, Neville AC. 1972 Quantitative studies on fibril orientation in beetle endocuticle. *J. Insect Physiol.* **18**. (doi:10.1016/0022-1910(72)90243-0)

40. Cheng L, Thomas A, Glancey JL, Karlsson AM. 2011 Mechanical behavior of bio-inspired laminated composites. *Compos. Part A Appl. Sci. Manuf.* **42**, 211–220. (doi:10.1016/j.compositesa.2010.11.009)

41. Signetti S, Pugno NM. 2014 Evidence of optimal interfaces in bio-inspired ceramic-composite panels for superior ballistic protection. *J. Eur. Ceram. Soc.* **34**, 2823–2831. (doi:10.1016/j.jeurceramsoc.2013.12.039)

42. Klocke D, Schmitz H. 2011 Water as a major modulator of the mechanical properties of insect cuticle. *Acta Biomater.* **7**, 2935–42. (doi:10.1016/j.actbio.2011.04.004)